Electronic supplementary information

Space conjugation induced white light and room-temperature phosphorescence from simple organic small molecule: Single-component WLED driven by both UV and blue chips

Xin Zheng[a], Yuanshan Huang[a], Duoduo Xiao[b], Shuming Yang[a], Zhenghuan Lin*[a] and Qidan Ling[c]

[a] *Fujian Key Laboratory of Polymer Materials, College of Chemistry and Materials Science, Fujian Normal University, Fuzhou 350007, China.*
E-mail: zhlin@fjnu.edu.cn
[b] *College of Chemistry, Guangdong University of Petrochemical Technology, Maoming 525000, China.*
[c] *Fujian Provincial Key Laboratory of Advanced Materials Oriented Chemical Engineering, Fuzhou, 350007, China*

EXPERIMENTAL SECTION

General methods.

UV-visible absorption spectra of the dilute solution were measured by a Shimadzu UV-2600 spectrophotometer. Fluorescence spectra of the solution and crystal were obtained on an Edinburgh Instruments FS5 Steady State Fluorescence Spectrofluorometer. NMR spectra were measured in DMSO-*d6* on a Bruker Ascend 400 FT-NMR at room temperature. ^{1}H NMR and ^{13}C NMR chemical shifts were quoted relative to the internal standard tetramethysilane. Photoluminescence absolute quantum yield (Φ) of the products was obtained at the room temperature using an Edinburgh Instruments FS5 Steady State Fluorescence Spectrofluorometer equipped with a 6-inch integrating sphere. Time-resolved fluorescence measurements were carried out using time-correlated single photon counting (TCSPC) spectrometer (Edinburgh Instruments FLS920) with an Edinburgh nF920 ultrafast nanosecond or microsecond flash lamp as the excitation source. Particle size was obtained at Malvern Zetasizer Nano ZSE.

Materials

All reagents and solvents obtained from commercial suppliers were directly used without further purification unless otherwise stated. TAD and TIM were synthesized according to the reported procedure. [1-2]

TAD. Beige solid: Yield 85%. ^{1}H NMR (400MHz, DMSO-*d6*) δ 8.65 (s,2H); ^{13}C NMR (101MHz, DMSO-*d6*) δ 157.44, 134.97, 131.91.

TIM. Yellow solid: Yield 68.3%. ^{1}H NMR (400MHz, DMSO-*d6*) δ 11.26 (s, 1H), 8.28 (s, 2H); ^{13}C NMR (101MHz, DMSO-*d6*) δ 163.74, 137.62, 127.77.

X-ray crystallography

The single crystals of **TAD** and **TIM** were mounted on a glass fiber for the X-ray diffraction analysis. Data sets were collected on an Agilent Technologies SuperNova single crystal diffractometer equipped with a graphite monochromated Mo-$K\alpha$ radiation (λ = 1.54184 Å) from a rotating anode generator at 100 K. Intensities were corrected for Lorentz-Polarization (*LP*) factors and empirical absorption using the ω scan technique. The structures were solved by direct methods and refined on F^2 with full matrix least-squares techniques using Siemens SHELXTL version 5 package of crystallographic software. Crystallographic data for their structure have been deposited

in the Cambridge Crystallographic Data Centre as supplementary publication no. CCDC 2062868 (for TAD) and 2062869 (for TIM).

Computational Methods

Theory calculations were performed with the Gaussian 09 program package. The geometries at ground state were optimized by the density functional theory (DFT) method with the Becke three-parameter hybrid exchange and the Lee-Yang-Parr correlation functional (B3LYP) and 6-31G* basis set. The excited state transition configurations were revealed by time-dependent (TD-B3LYP) using 6-31G* basis sets.

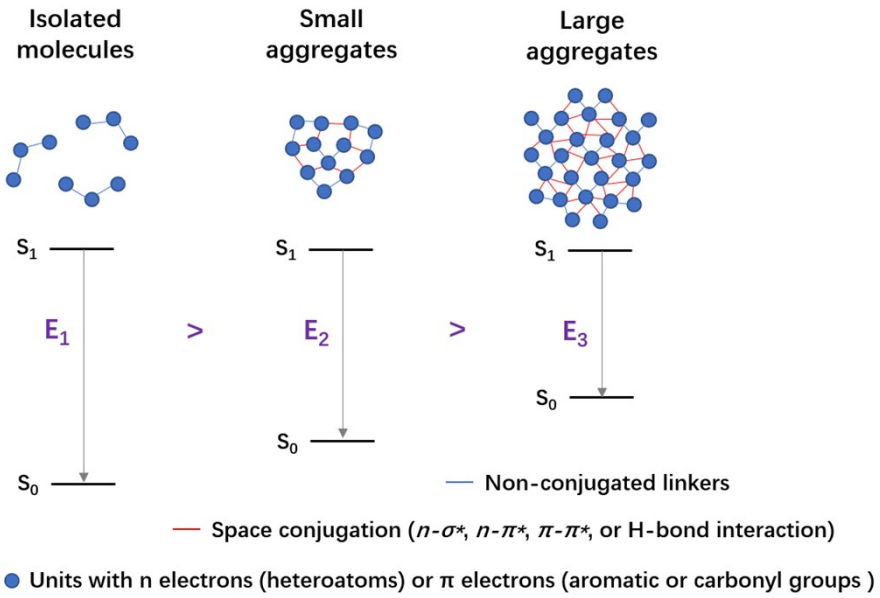

Fig. S1 Schematic illustration of the effect of space conjugation (SC) on emission of nontraditional fluorophores.

Table S1 Properties of single-component white light emitting materials based on small organic molecules.

Organic dye	Molecular weight	Φ (%)	CIE (x, y)	CRI	CCT (K)	Ref.
TAD	154	26.8	0.26, 0.30			This work
TIM	153	11.8	0.33, 0.35	85	5669	
1	189	2	0.31, 0.35	83	6218	3
TPO-Br	454		0.31, 0.33			4
PTZ-Ph-TTR	477	11	0.33, 0.33	92		5
2PQ−PTZ	479		0.32, 0.34	89	5850	6
rac-BINAP	622	7.6	0.37, 0.44	73		7
CTM	453		0.35, 0.35	88.8		8
D1c	356	32	0.34, 0.36			9
Cz9PhAn	660	47	0.30, 0.33	75.6		10
2	293	16	0.31, 0.34			11
OPC	544	23	0.35, 0.35			12
PTZ-BP	379	8	0.28, 0.30			13
DPPZ	280	1	0.28, 0.33			14
ClBDBT	322	7.2	0.33, 0.35			15
ImBr	369	4.1	0.29, 0.35			16
3-DPH-XO	363	40	0.27, 0.35			17
SDB2t	582	13	0.27, 0.27			18
P3	310	36	0.28, 0.31			19

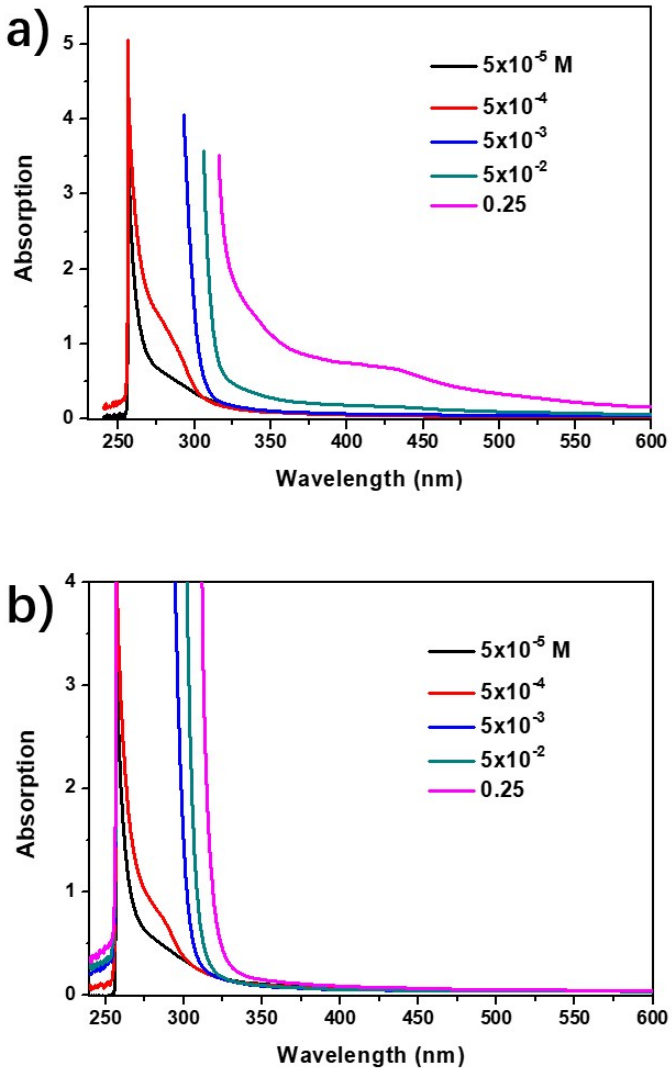

Fig. S2 Absorption of TIM (a) and TAD (b) in DMF solution at different concentration.

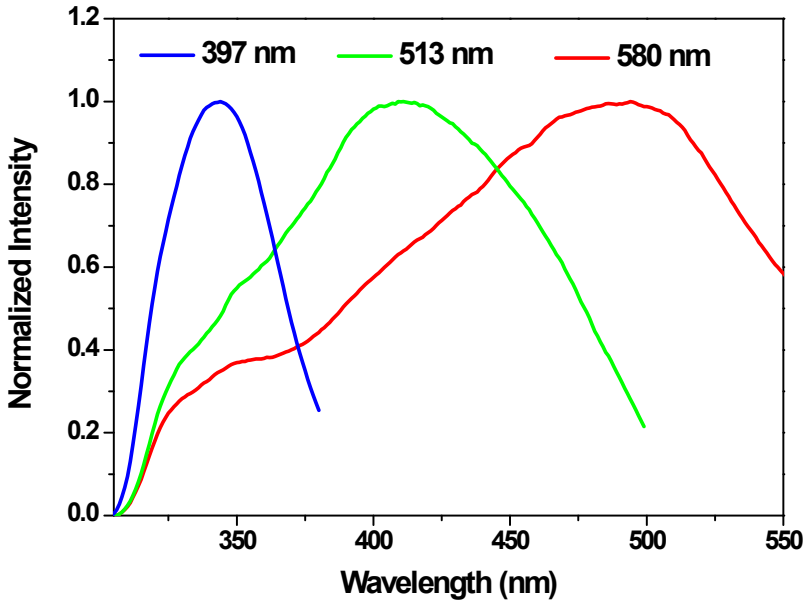

Fig. S3 Excitation spectra monitored at different emissive peaks (397 nm, 513 nm and 580 nm) of TIM solution at 0.25 M.

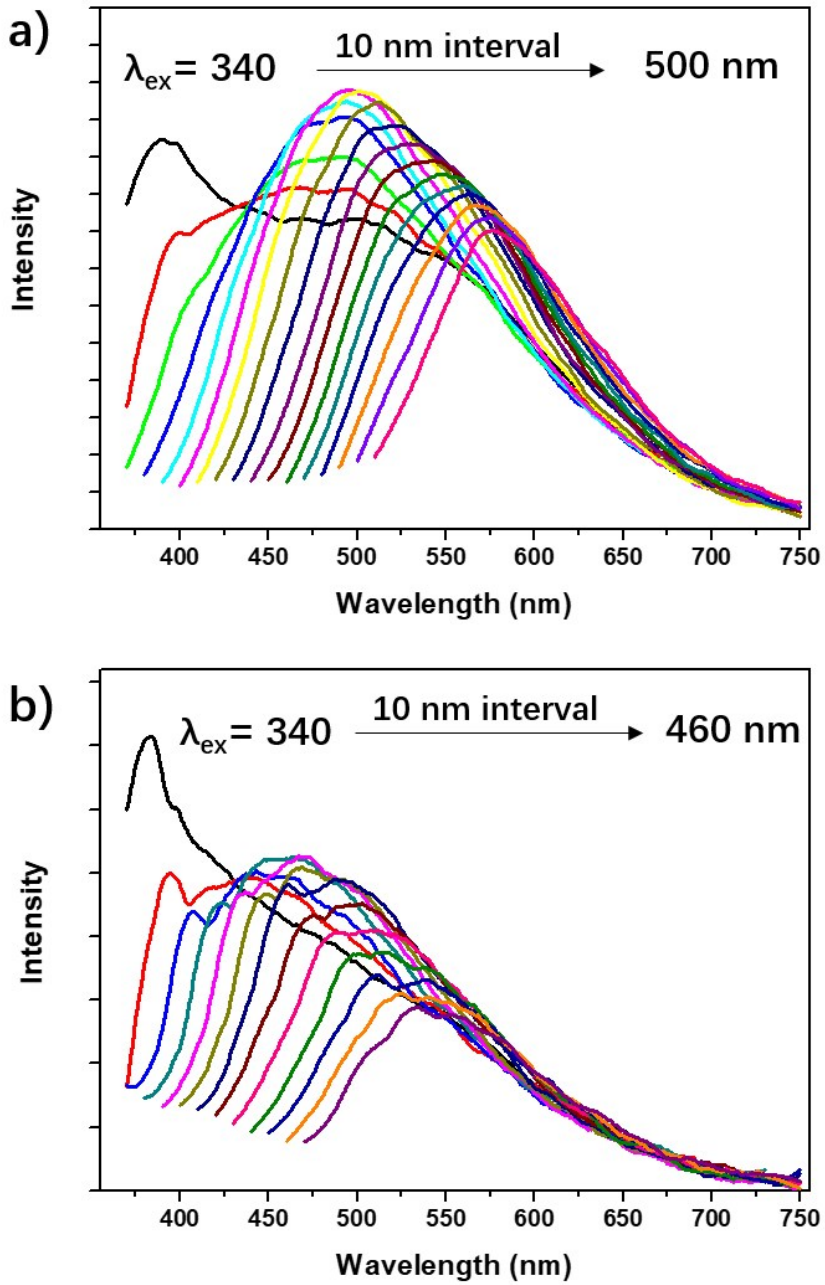

Fig S4 Emission spectra of $5x10^{-2}$ M (a) and $5x10^{-3}$ M (b) solution excited at different wavelength.

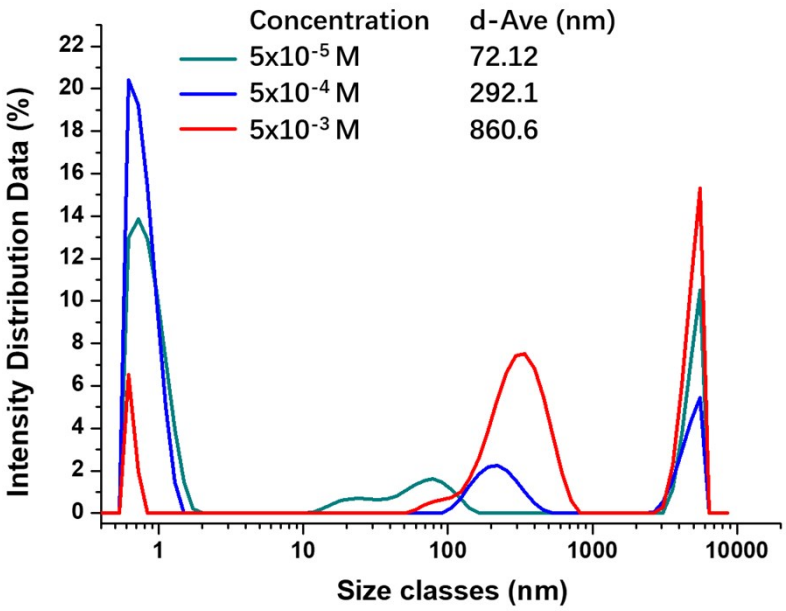

Fig. S5 Particle size distribution curves and average particle size of TIM in solution with different concentration.

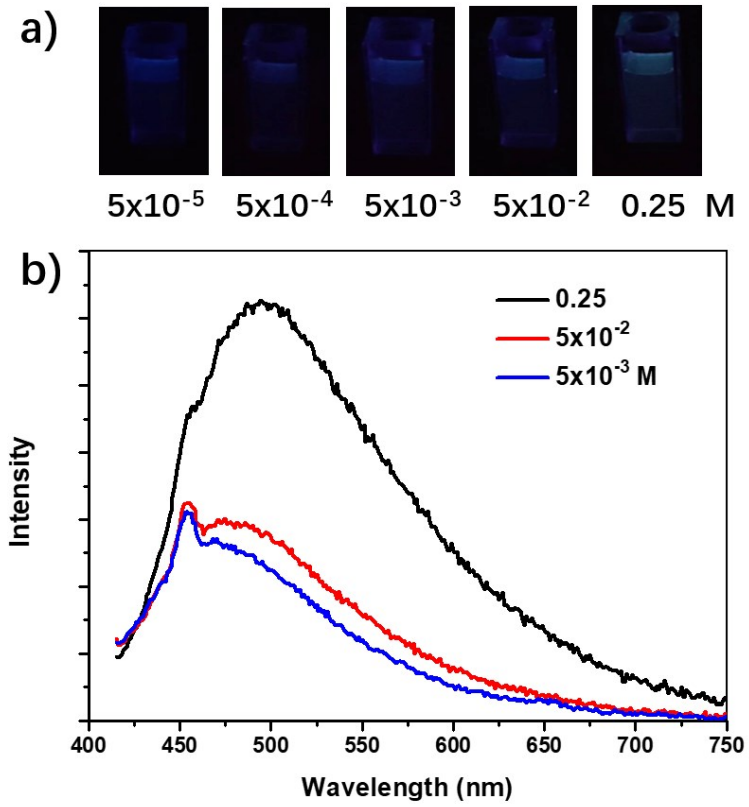

Fig S6 Optic properties of TAD in solution at different concentration: a) Photos under 365 nm of UV lamp; b) Emission spectra under excitation at 398 nm.

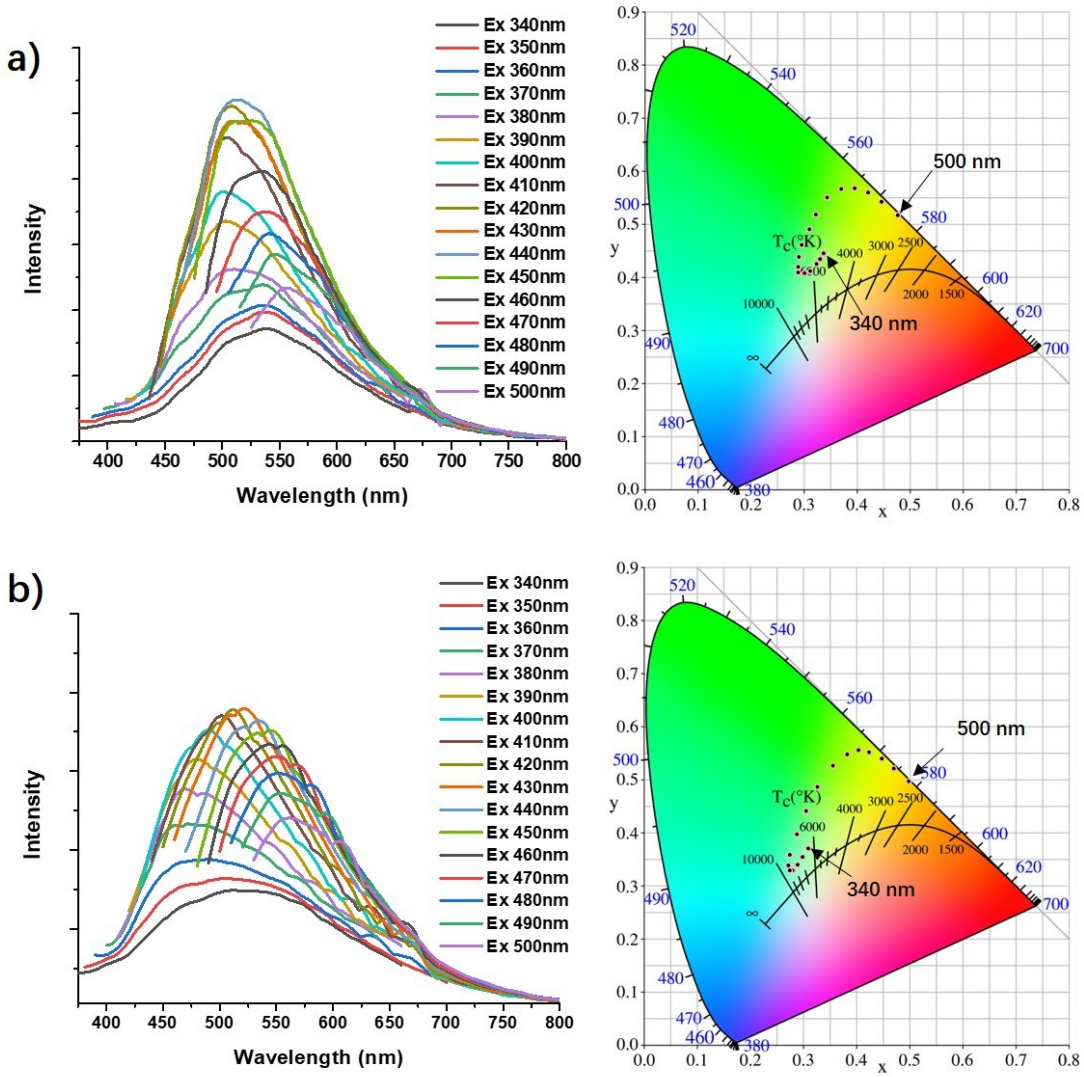

Fig S7 Emission spectra (Left) and CIE coordination value (Right) of TIM (a) and TAD (b) crystals excited at different wavelength.

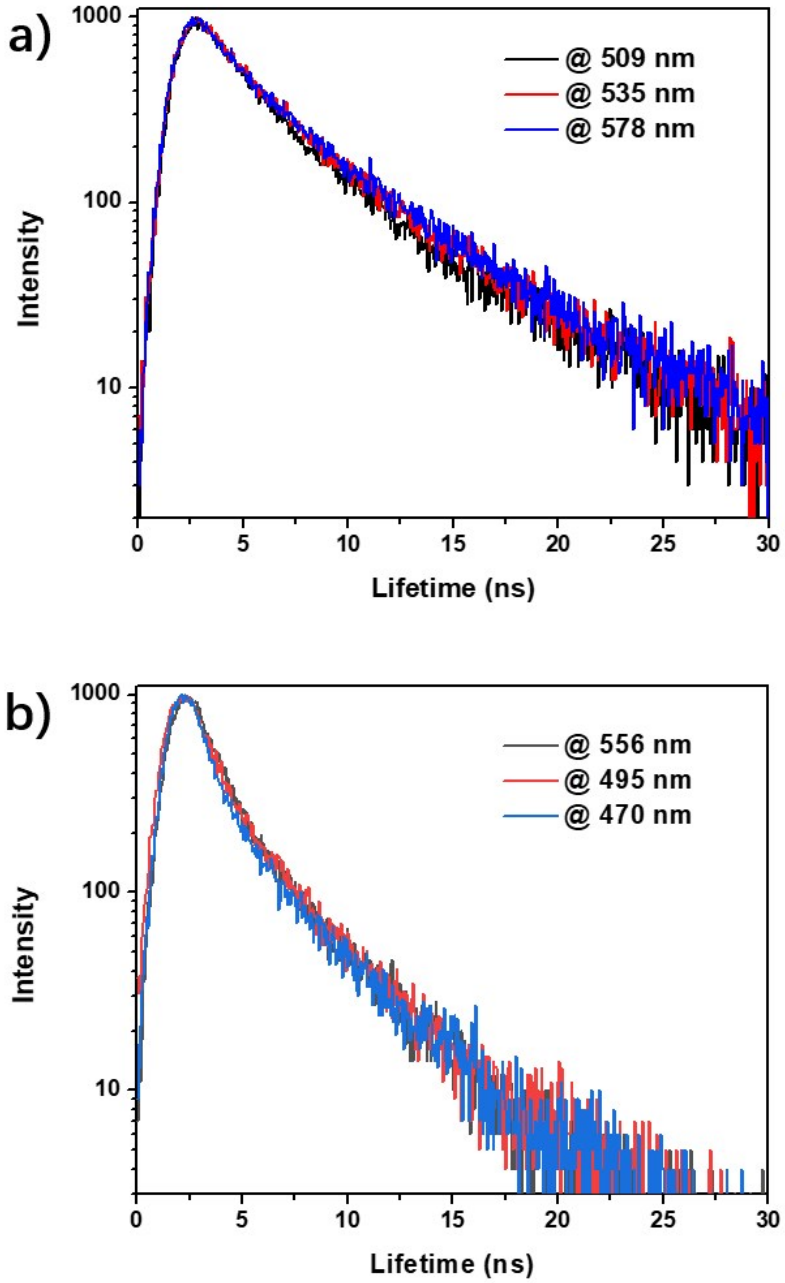

Fig S8 Transient luminescence delay curves of TIM (a) and TAD (b).

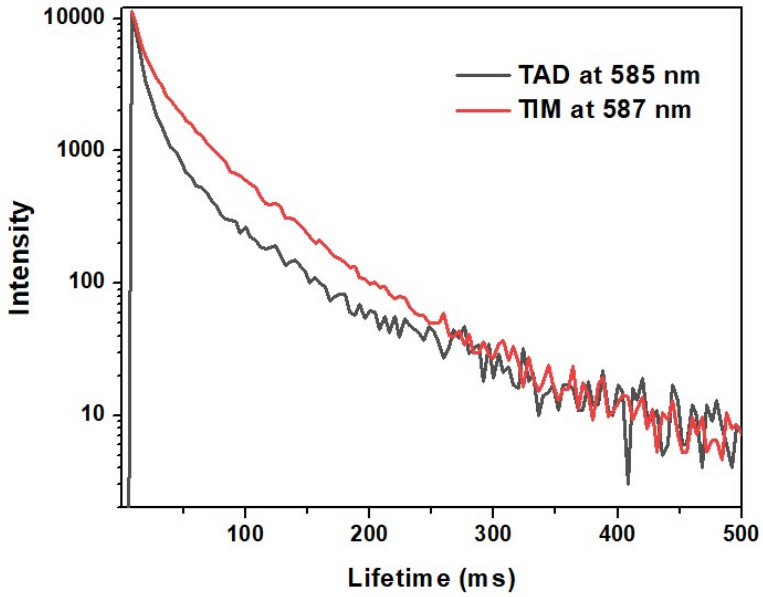

Fig S9 Transient luminescence delay curves of TIM (a) and TAD (b).

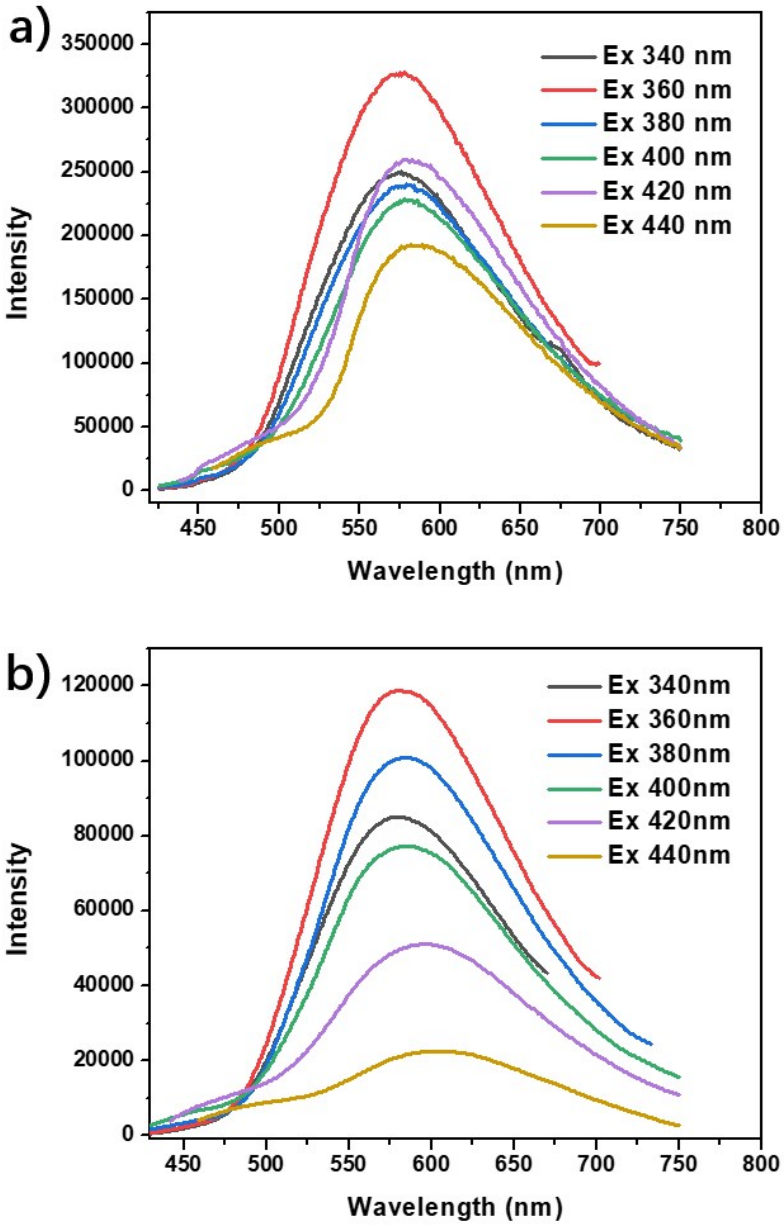

Fig S10 Phosphorescence spectra of TIM (a) and TAD (b) crystals under different excitation wavelength.

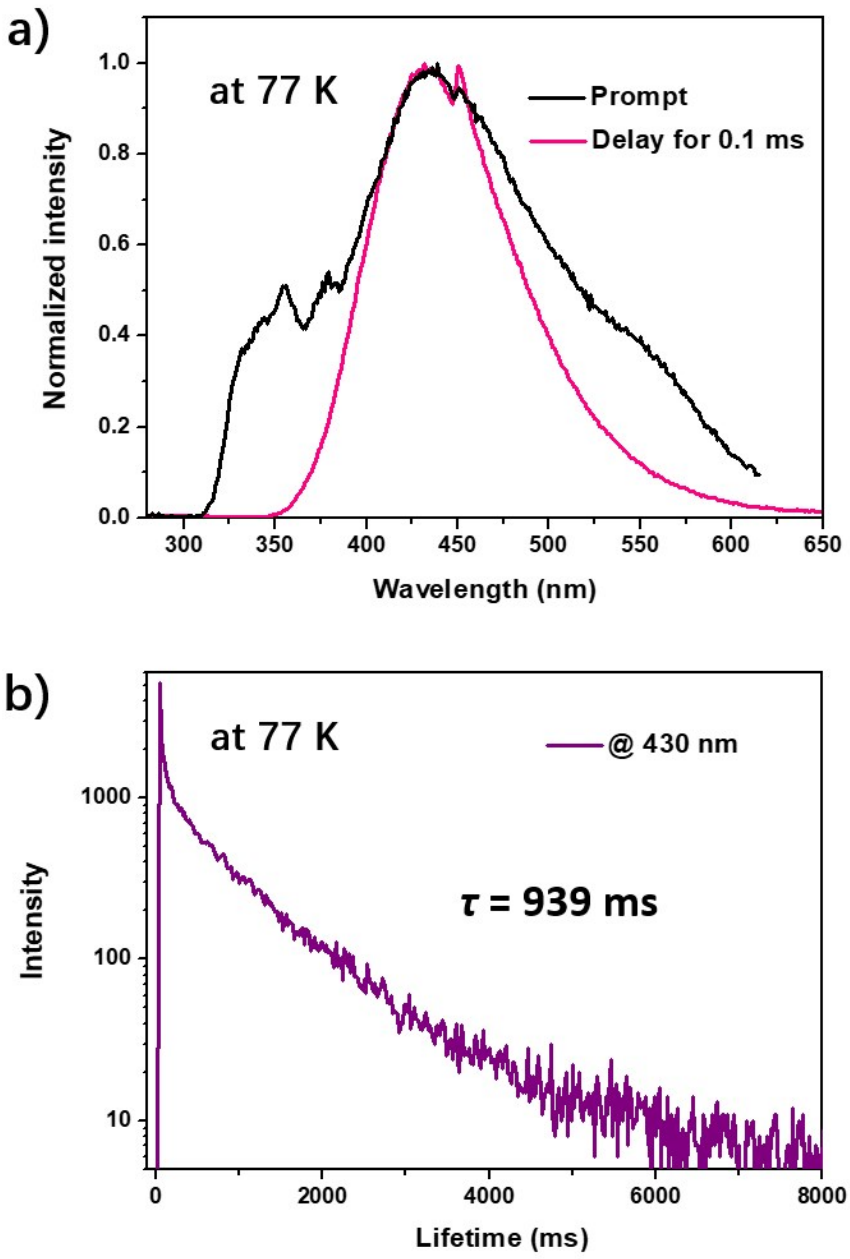

Fig S11 Prompt and delay emission spectrum (a) and transient luminescence curve (b) of TIM in dilute solution (1×10^{-6} M) at 77K.

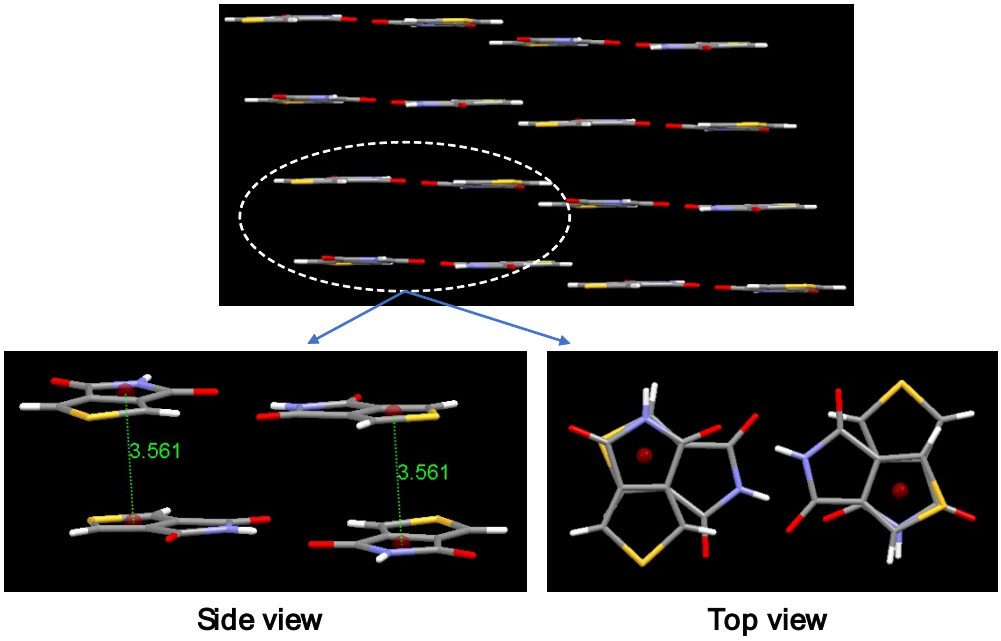

Fig S12 Layered structure and interlayer interaction of TIM crystal.

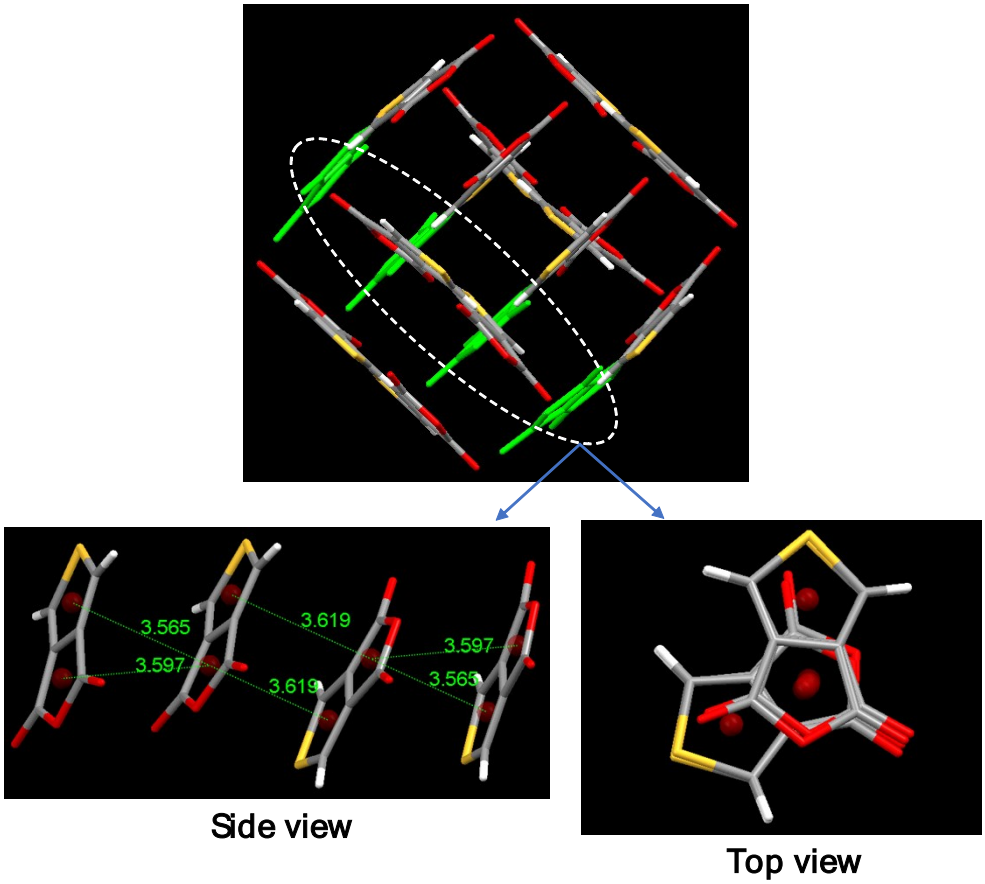

Fig S13 Packing structure and intermolecular interaction of TAD crystal.

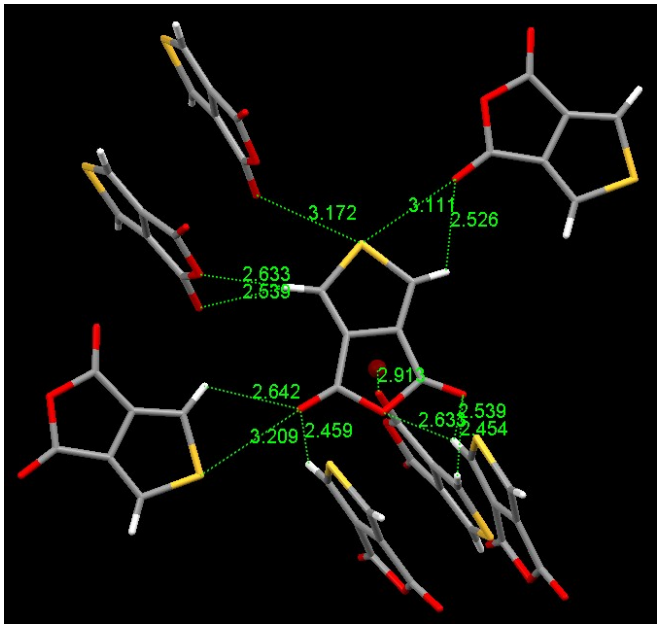

Fig S14 Intermolecular interaction of TAD crystal.

Table S2 Crystal data and structure refinement for TIM and TAD.

Crystal	TIM	TAD
Formula	$C_6H_3NO_2S$	$C_{12}H_4O_6S_2$
Formula weight	153.15	308.27
Shape	block	block
Crystal system	monoclinic	tetragonal
Space group	P 21/c	$P4_12_12$
a (Å)	10.920(4)	10.1007(5)
b (Å)	7.869(3)	10.1007(5)
c (Å)	7.186(4)	23.3207(16)
α(deg)	90.00	90.00
β(deg)	94.531(6)	90.00
γ(deg)	90.00	90.00
V ($Å^3$)	615.6(4)	2379.3(3)
Z	4	8
$D_{calcd.}(g/cm^3)$	1.653	1.721
F(000)	312	1248
R (int)	0.0373	0.0243
GOF on F^2	1.002	1.021
R1[I > 2σ(I)]	0.0413	0.0211
wR2[I>2σ(I)]	0.0866	0.0544
R1 (all data)	0.0624	0.0232
wR2(all data)	0.0928	0.0557

Table S3 TDDFT computed absorption and emission properties of TIM and TAD monomer

Monomer	**Transition**	**Excited state**	**Main orbital transition[a] (CIC)**	***E*, eV**	***λ*, nm**	***f***
TIM	Absorption	S_4	HOMO-2→LUMO+1 (0.31) HOMO→LUMO (0.63)	4.86	255	0.0198
	Emission	S_1	LUMO+1→HOMO-3 (0.10) LUMO→HOMO (0.70)	3.46	358	0.0001
TAD	Absorption	S_3	HOMO-2→LUMO+1 (0.35) HOMO→LUMO (0.61)	4.92	252	0.0125
	Emission	S_1	LUMO→HOMO (-0.68) LUMO+1→HOMO (0.18)	3.28	378	0.0001

[a] CI expansion coefficients for the main orbital transitions.

Table S4 TDDFT computed excited-state data of monomer and different aggregates of TIM.

Type	Excited state	Main orbital transition[a] (CIC)	λ, nm	f
Monomer	S_4	HOMO-2→LUMO+1 (0.31)	255	0.0198
		HOMO→LUMO (0.63)		
	S_7	HOMO→LUMO+1 (0.69)	224	0.0405
	S_9	HOMO-4→LUMO+1 (-0.44)	209	0.3262
		HOMO-2→LUMO+1 (0.45)		
		HOMO→LUMO (-0.27)		
CH-Tetramer	S_4	HOMO-3→LUMO+2 (0.37)	296	0.0002
		HOMO-2→LUMO+3 (0.37)		
	S_9	HOMO-6→LUMO+2 (-0.30)	262	0.0033
		HOMO-1→LUMO (0.48)		
	S_{19}	HOMO-1→LUMO+3 (0.41)	257	0.1040
		HOMO→LUMO+2 (0.42)		
NH-Tetramer	S_2	HOMO-8→LUMO (-0.29)	297	0.0002
		HOMO-8→LUMO+1 (0.63)		
	S_7	HOMO-1→LUMO (0.66)	273	0.0010
		HOMO-1→LUMO+1 (0.25)		
	S_{19}	HOMO-6→LUMO (0.44)	259	0.0493
		HOMO-4→LUMO+1 (0.20)		
ππ-Tetramer	S_1	HOMO-6→LUMO (0.43)	305	0.0007
		HOMO-4→LUMO (0.23)		
	S_9	HOMO-2→LUMO (0.49)	270	0.0041
		HOMO-1→LUMO+1 (0.26)		
	S_{14}	HOMO-5→LUMO (-0.28)	261	0.0048
		HOMO-5→LUMO+1 (0.33)		
M-Tetramer	S_1	HOMO-1→LUMO+3 (0.33)	303	0.0004
		HOMO→LUMO+2 (0.27)		
	S_7	HOMO-3→LUMO (0.41)	272	0.0140
		HOMO-2→LUMO+1 (-0.39)		
	S_{17}	HOMO-3→LUMO+3 (0.30)	262	0.0102
		HOMO-2→LUMO+2 (-0.26)		

[a] CI expansion coefficients for the main orbital transitions.

Table S5 TDDFT computed excited-state data of monomer and different aggregates of TAD.

Type	Excited state	Main orbital transition[a] (CIC)	λ, nm	*f*
Monomer	S_3	HOMO-2→LUMO+1 (0.35) HOMO→LUMO (0.61)	252	0.0125
	S_7	HOMO-2→LUMO (0.28) HOMO→LUMO+1 (0.63)	228	0.0708
	S_8	HOMO-2→LUMO+1 (0.59) HOMO→LUMO (-0.35)	209	0.4589
πO-Dimer	S_5	HOMO-5→LUMO+2 (0.25) HOMO→LUMO (0.58)	254	0.0303
	S_8	HOMO-1→LUMO+1 (0.56) HOMO→LUMO+1 (-0.24)	245	0.0098
	S_{20}	HOMO-1→LUMO+2 (0.45) HOMO→LUMO+2 (-0.34)	226	0.0920
HO-Dimer	S_3	HOMO→LUMO (0.69)	277	0.0023
	S_9	HOMO-3→LUMO (0.46) HOMO-2→LUMO (0.33)	251	0.0167
	S_{20}	HOMO-3→LUMO+1 (0.52) HOMO→LUMO+3 (0.26)	225	0.1017
ππ-Dimer	S_1	HOMO→LUMO+3 (0.64)	290	0.0004
	S_7	HOMO-1→LUMO (0.33) HOMO-1→LUMO+1 (0.53)	259	0.0138
	S_{12}	HOMO-2→LUMO (0.31) HOMO-1→LUMO+2 (0.35)	242	0.0169
OS-Dimer	S_3	HOMO→LUMO (0.68)	278	0.0007
	S_{10}	HOMO-2→LUMO+3 (-0.34) HOMO→LUMO+2 (0.60)	251	0.0192
	S_{18}	HOMO-3→LUMO+1 (0.530) HOMO→LUMO+3 (-0.34)	225	0.1104
Tetramer	S_2	HOMO→LUMO+1 (0.54) HOMO→LUMO+2 (0.37)	311	0.0013
	S_3	HOMO→LUMO+1 (0.45) HOMO→LUMO+2 (-0.41)	307	0.0008
	S_7	HOMO-3→LUMO (0.70)	295	0.0034

[a] CI expansion coefficients for the main orbital transitions.

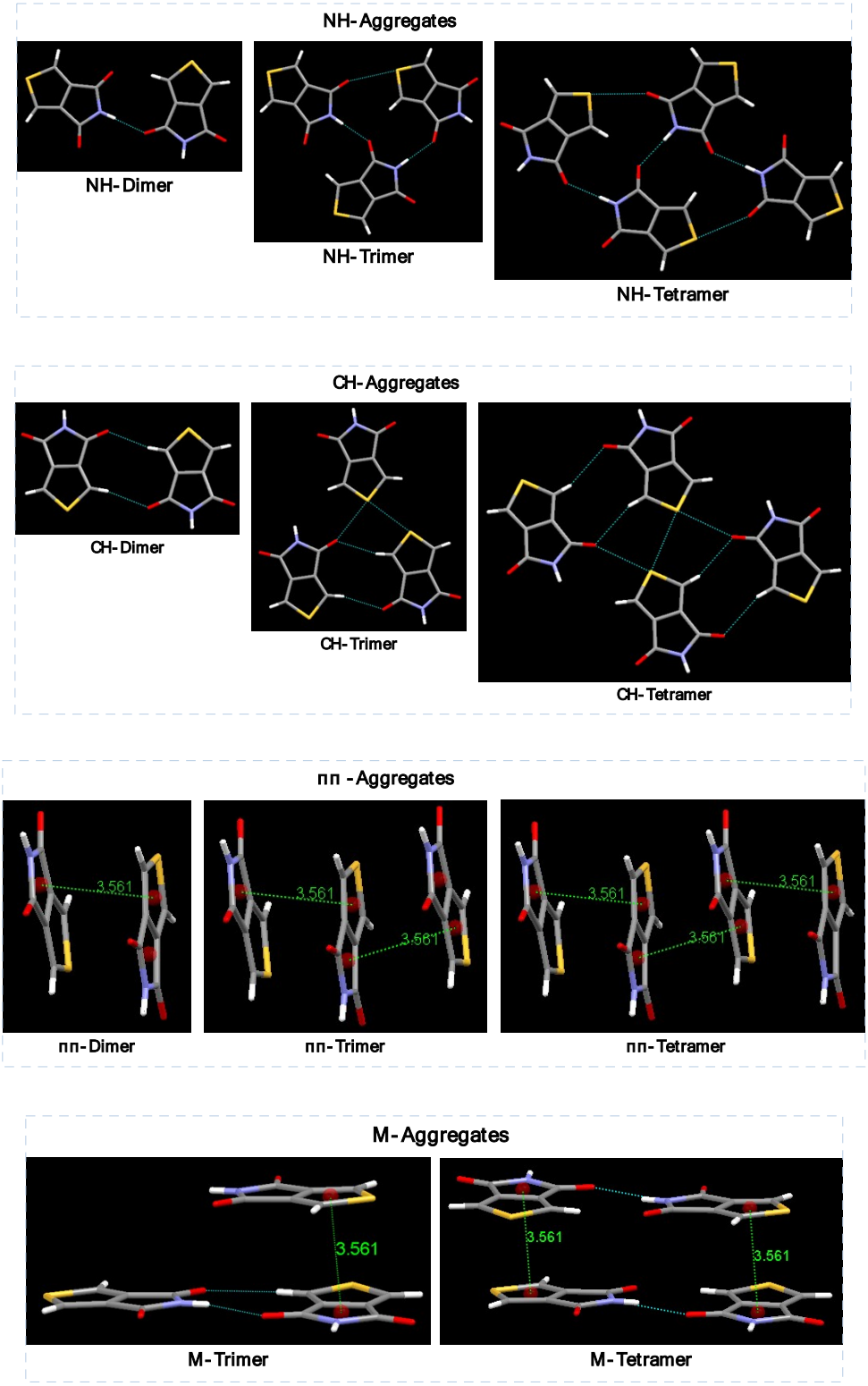

Fig. S15 Different aggregates in TIM crystals.

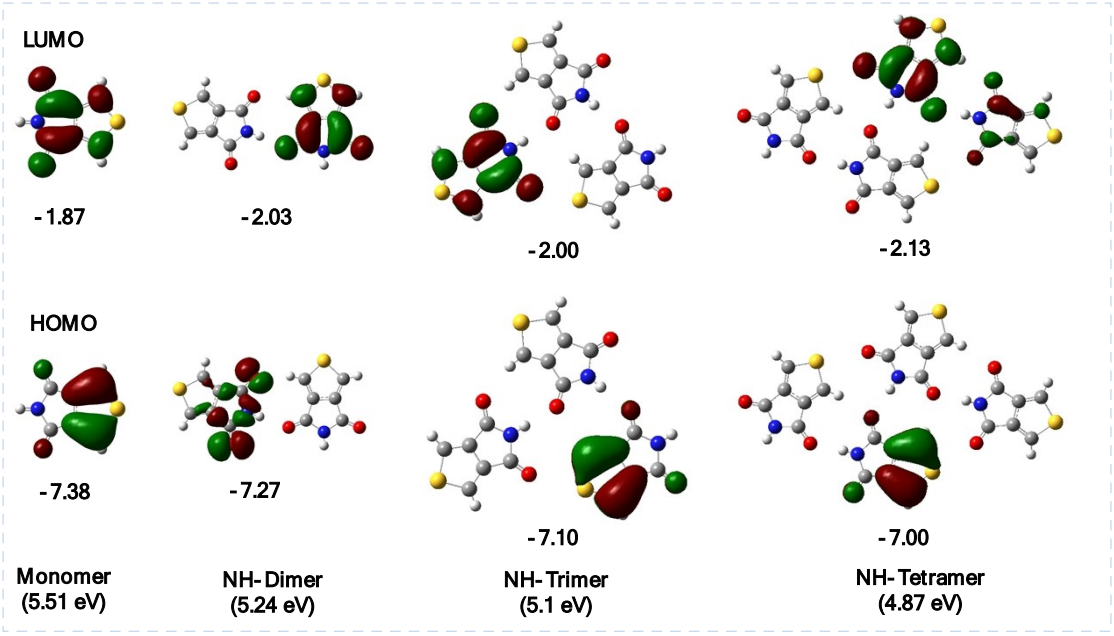

Fig. S16 Calculated frontier orbitals of different NH-aggregates in TIM crystals.

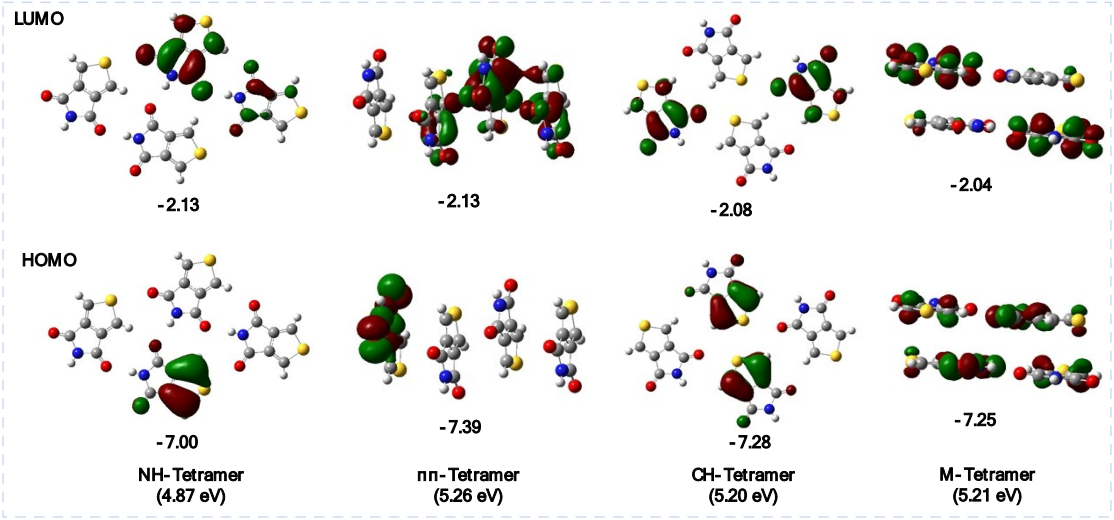

Fig. S17 Calculated frontier orbitals of different tetramers in TIM crystals.

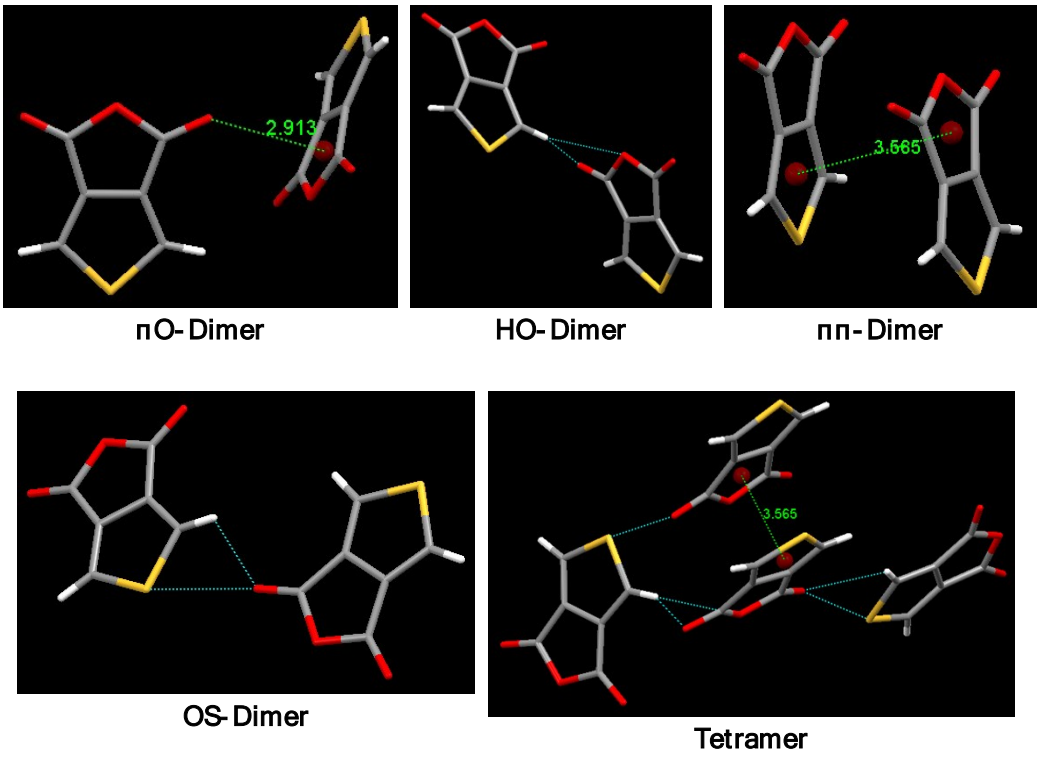

Fig. S18 Different aggregates in TAD crystals.

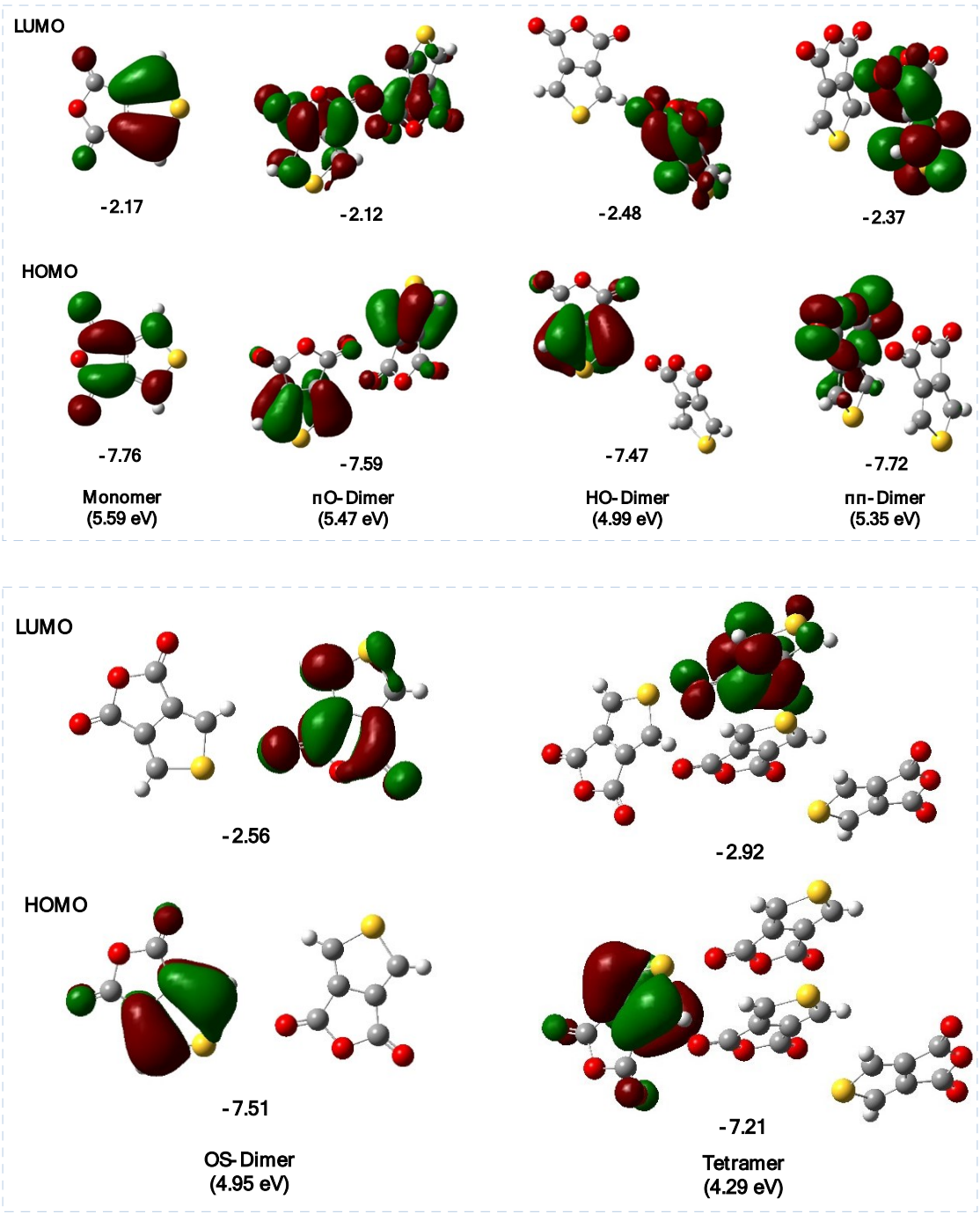

Fig. S19 Calculated frontier orbitals of different tetramers in TAD crystals.

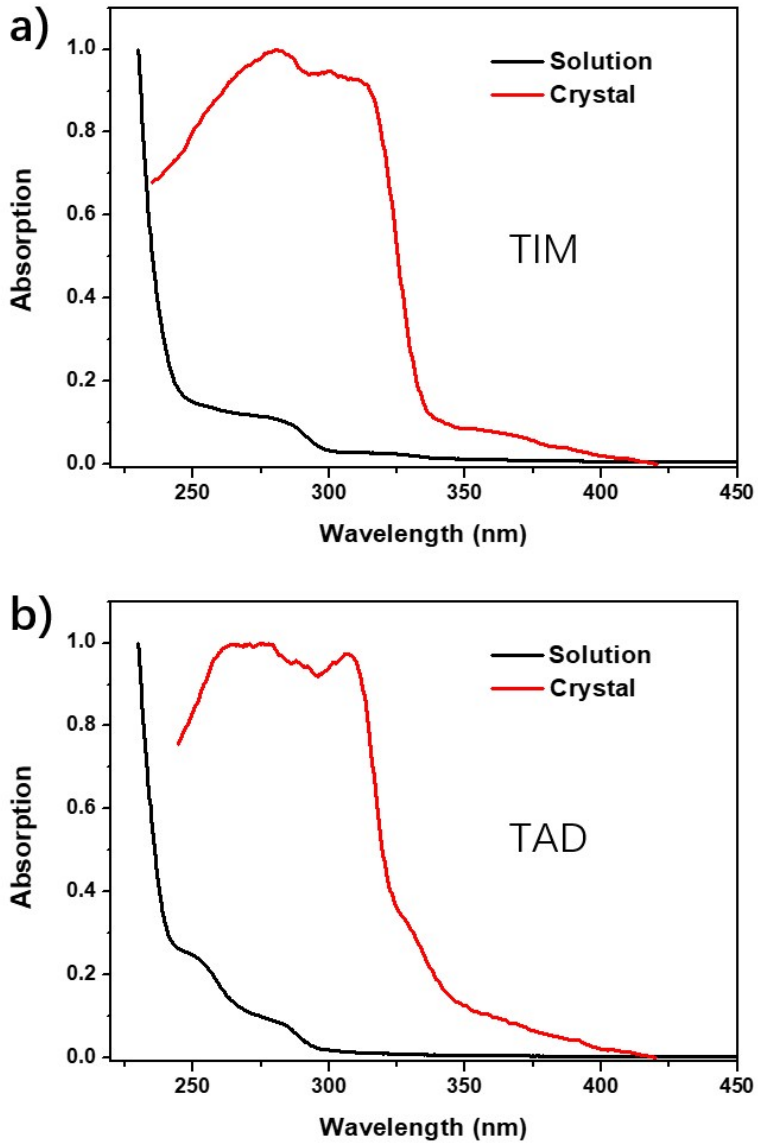

Fig. S20 Absorption spectra of TIM (a) and TAD (b) in dilute chloroform solution and crystals.

Table S6 Calculated singlet-triplet energy gap for TIM and TAD

Compound	Type	$E(S_1)$, eV	$E(T_1)$, eV	ΔE_{ST}, eV
TIM	Monomer	4.13	3.34	0.79
	CH-Tetramer	4.18	3.45	0.73
	NH-Tetramer	4.16	3.46	0.70
	ππ-Tetramer	4.07	3.40	0.67
	M-Tetramer	4.09	3.43	0.66
TAD	Monomer	4.39	3.25	1.14
	πO-Dimer	4.42	3.31	1.11
	HO-Dimer	4.33	3.30	1.03
	ππ-Dimer	4.28	3.29	0.99
	OS-Dimer	4.39	3.33	1.06
	Tetramer	3.80	3.30	0.5

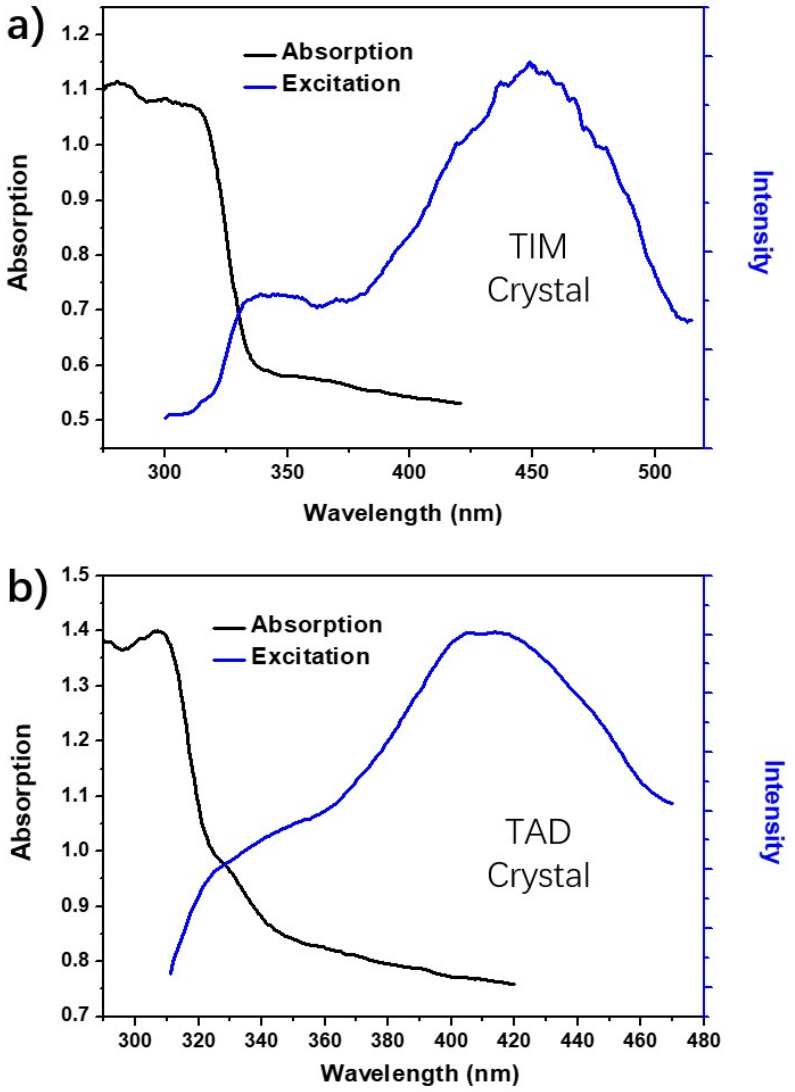

Fig. S21 Comparison of absorption and excitation spectra of TIM (a) and TAD (b) in crystals.

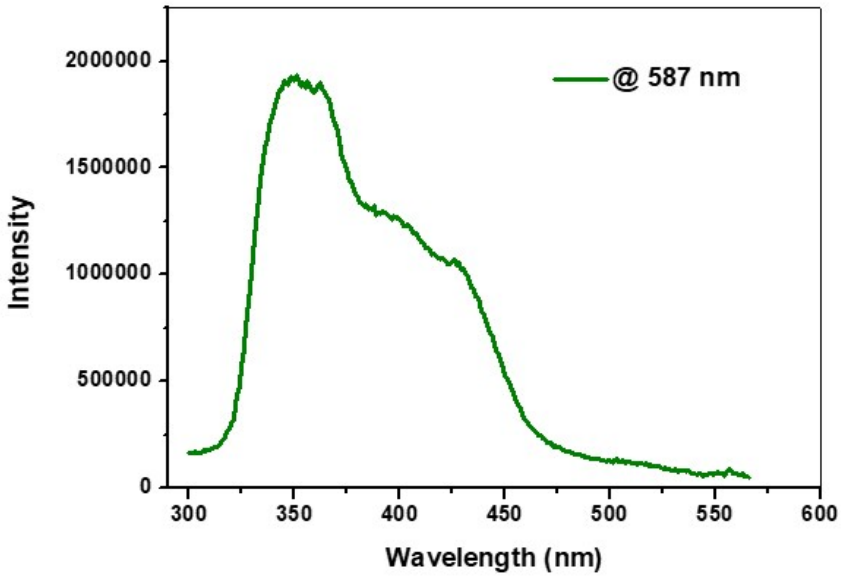

Fig. S22 Excitation spectrum of phosphorescence of TIM crystal.

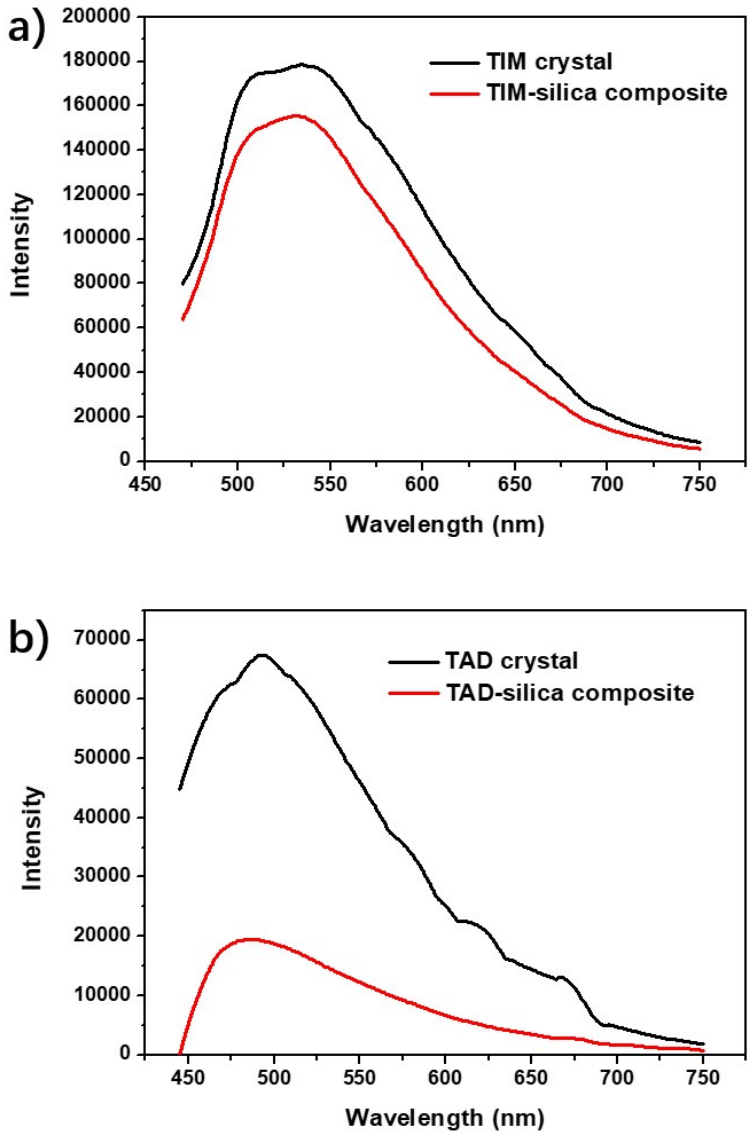

Fig S23 Comparison of luminous intensity of TIM (a) and TAD (b) crystals with their silica composites.

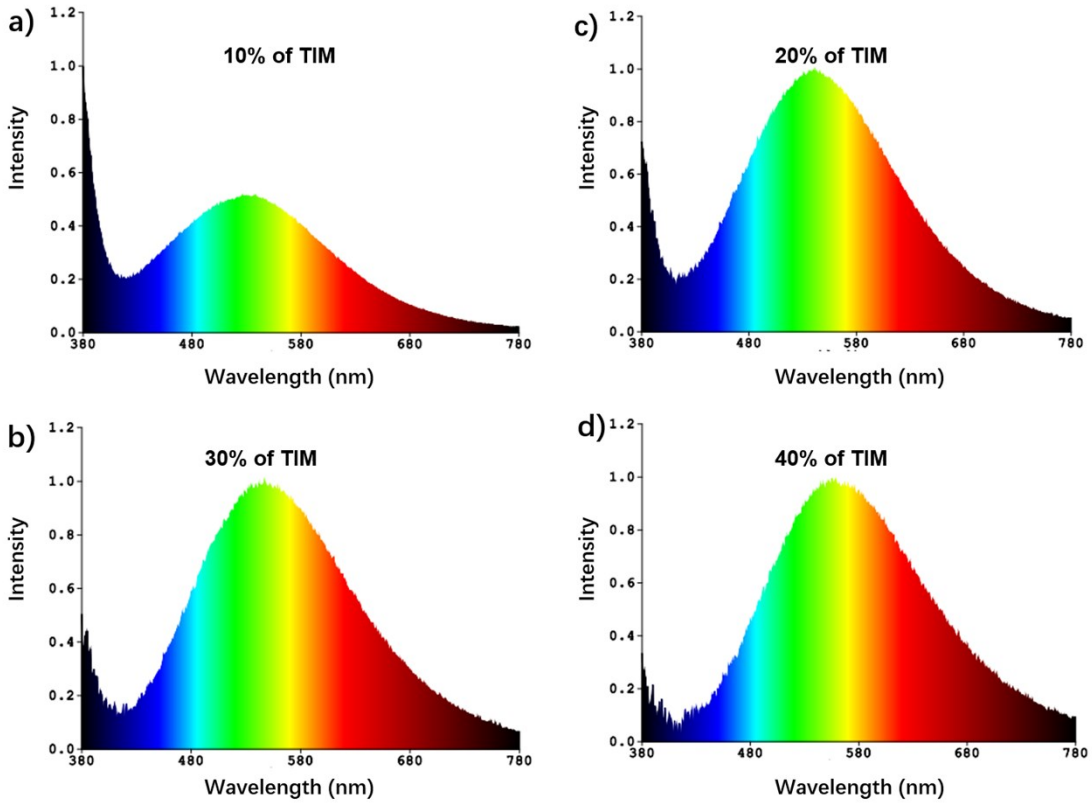

Fig S24 Electroluminescent spectra of UV chip-driven WLED based on different amount of TIM.

Table S7 Electroluminescent data of WLED devices driven by UV and blue chips.

Chip type	loading amount of TIM (%)	CIE (x, y)	CCT (K)	CRI
UV	10	0.31, 0.39	6239	75.4
	20	0.34, 0.43	5213	73.1
	30	0.36, 0.45	4779	72.8
	40	0.39, 0.46	4200	73.4
Blue	30	0.21, 0.18	100000	76.1
	40	0.25, 0.24	34040	89.0
	50	0.33, 0.35	5669	84.6

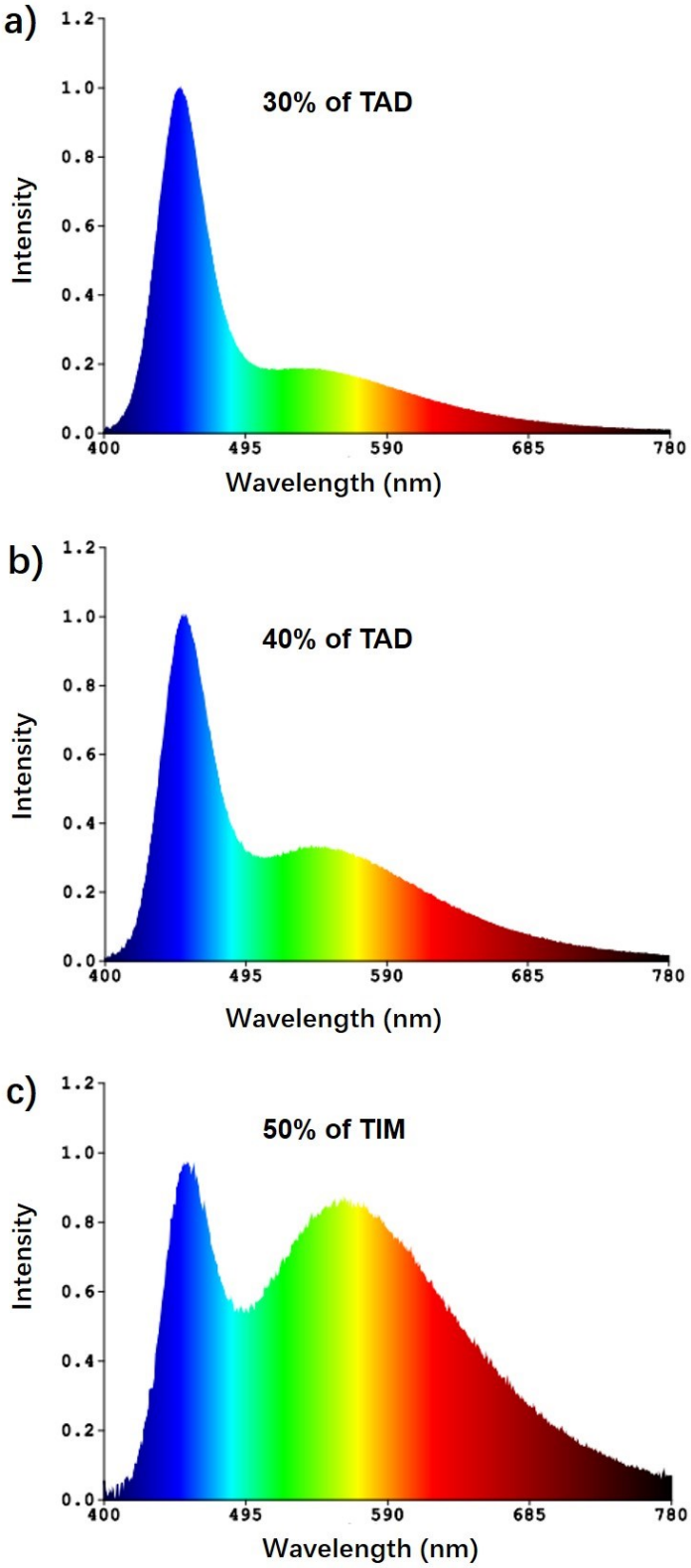

Fig S25 Electroluminescent spectra of blue chip-driven WLED based on different amount of TIM.

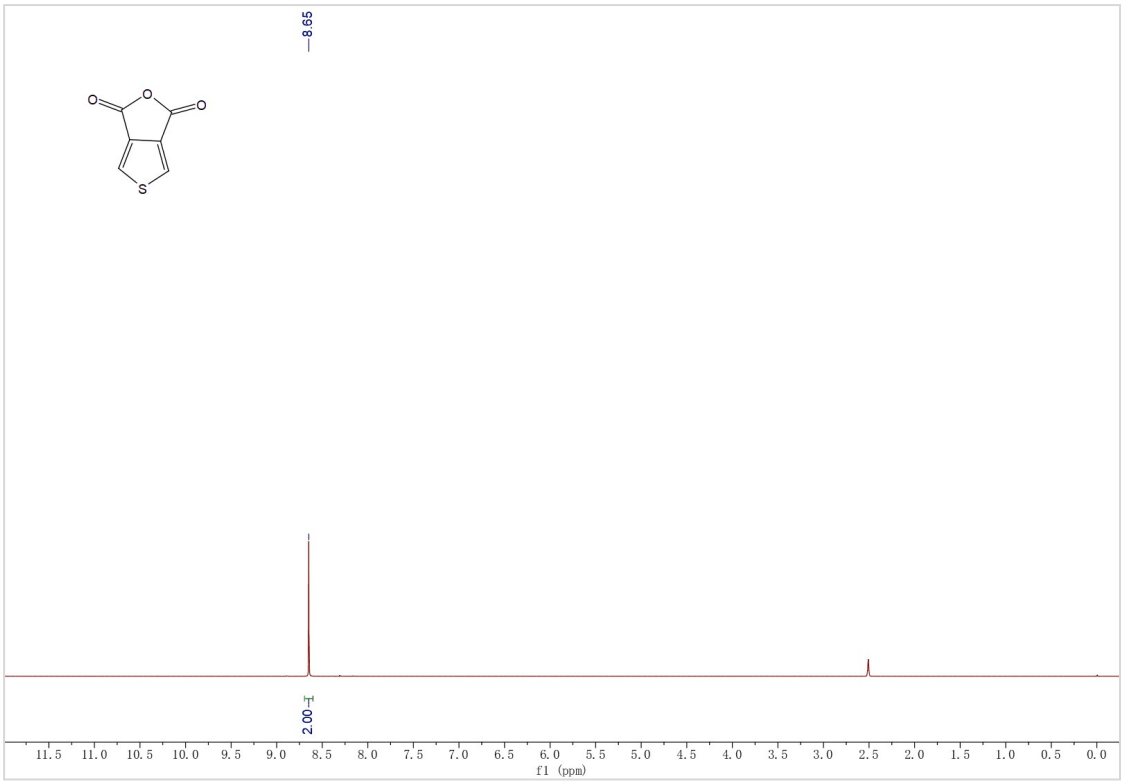

Fig S26 ^{1}H NMR spectrum of TAD.

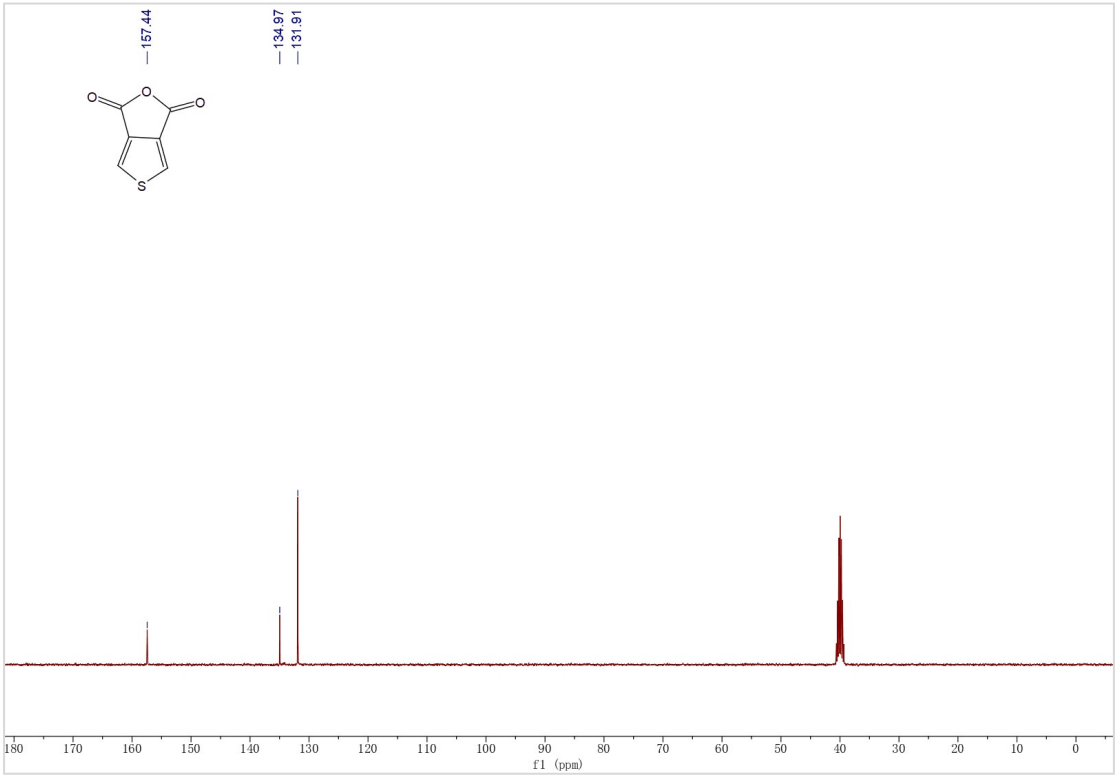

Fig S27 ^{13}C NMR spectrum of TAD.

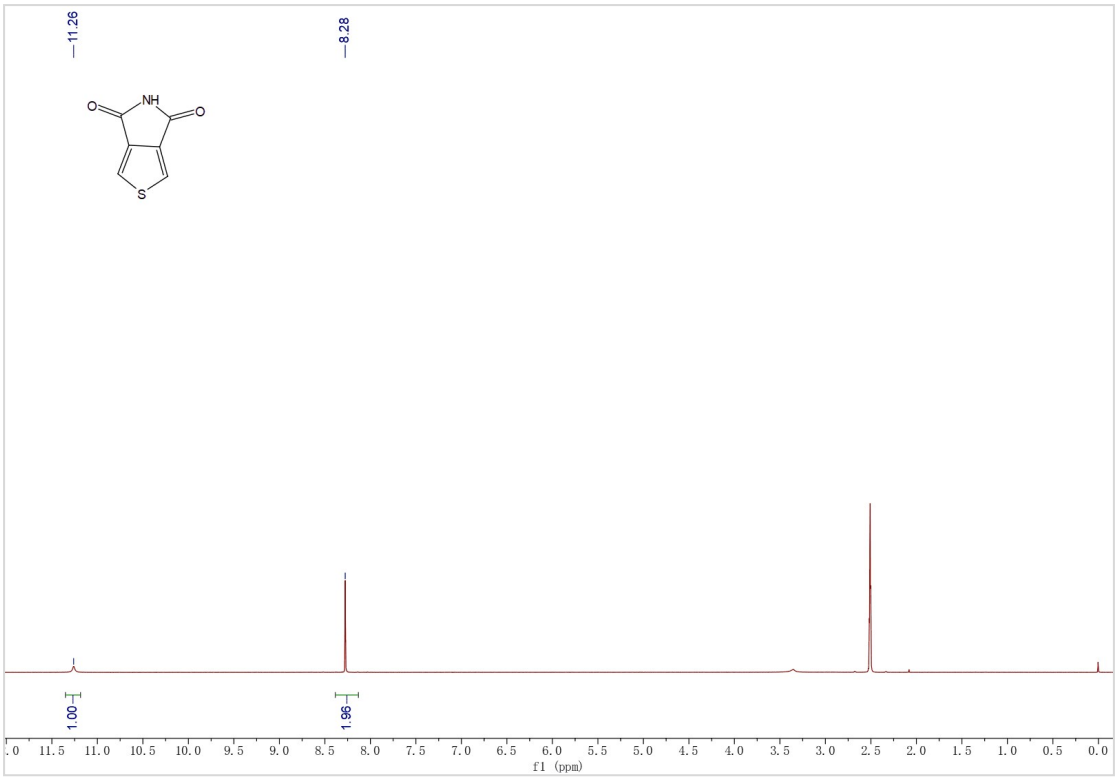

Fig S28 ^{1}H NMR spectrum of TIM.

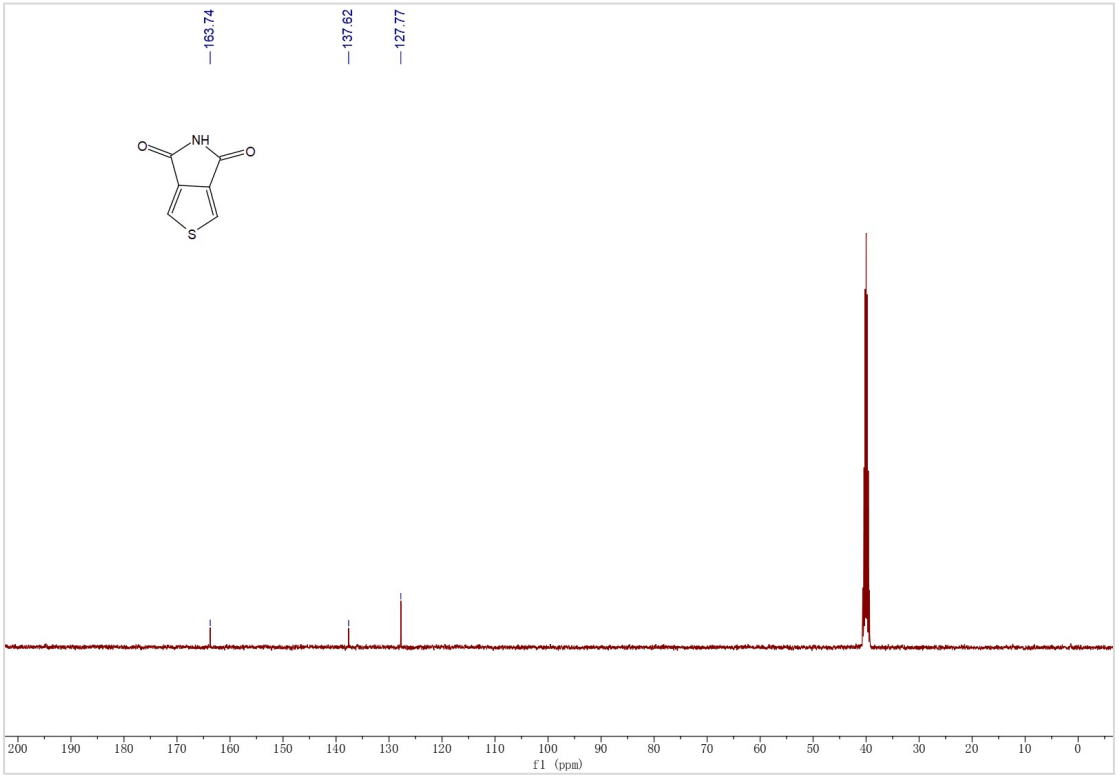

Fig S29 ^{13}C NMR spectrum of TIM.

Reference

[1] T. Weller, M. Breunig, C. J. Mueller, E. Gann, C. R. McNeill and M. Thelakkat, Fluorination in thieno[3,4-*c*]pyrrole-4,6-dione copolymers leading to electron transport, high crystallinity and end-on alignment. *J. Mater. Chem. C*, 2017, **5**, 7527-7534.

[2] R. M. W. Wolfe and J. R. Reynolds, Direct Imide Formation from Thiophene Dicarboxylic Acids Gives Expanded Side-Chain Selection in Thienopyrrolediones. *Org. Lett.,* 2017, **19**, 996−999.

[3] N. N. Zhang, C. Sun, X. M. Jiang, X. S. Xing, Y. Yan, L. Z. Cai, M. S. Wang and G. C. Guo, Single-component small-molecule white light organic phosphors, *Chem. Commun.*, 2017, **53**, 9269-9272.

[4] J. Wang, X. Gu, H. Ma, Q. Peng, X. Huang, X. Zheng, S. H. P. Sung, G. Shan, J. W. Y. Lam, Z. Shuai and B. Z. Tang, A facile strategy for realizing room temperature phosphorescence and single molecule white light emission, *Nat. Commun.*, 2018, **9**, 2963.

[5] K. Wang, Y. Z. Shi, C. J. Zheng, W. Liu, K. Liang, X. Li, M. Zhang, H. Lin, S. L. Tao, C. S. Lee, X. M. Ou and X. H. Zhang, Control of Dual Conformations: Developing Thermally Activated Delayed Fluorescence Emitters for Highly Efficient Single-Emitter White Organic Light-Emitting Diodes, *ACS Appl. Mater. Interfaces*, 2018, **10**, 31515-31525.

[6] B. Li, Z. Li, F. Guo, J. Song, X. Jiang, Y. Wang, S. Gao, J. Wang, X. Pang, L. Zhao and Y. Zhang, Realizing Efficient Single Organic Molecular White Light-Emitting Diodes from Conformational Isomerization of Quinazoline-Based Emitters, *ACS Appl. Mater. Interfaces*, 2020, **12**, 14233-14243.

[7] X. Wu, C. Y. Huang, D. G. Chen, D. Liu, C. Wu, K. J. Chou, B. Zhang, Y. Wang, Y. Liu, E. Y. Li, W. Zhu and P. T. Chou, Exploiting racemism enhanced organic room-temperature phosphorescence to demonstrate Wallach's rule in the lighting chiral chromophores, *Nat. Commun.*, 2020, **11**, 2145.

[8] J.-H. Tan, W.-C. Chen, S.-F. Ni, Z. Qiu, Y. Zhan, Z. Yang, J. Xiong, C. Cao, Y. Huo and C.-S. Lee, Aggregation-state engineering and emission switching in D–A–D′ AIEgens featuring dual emission, MCL and white electroluminescence, *J. Mater. Chem. C*, 2020, **8**, 8061-8068.

[9] Q. Y. Yang and J. M. Lehn, Bright white-light emission from a single organic compound in the solid state, *Angew. Chem. Int. Ed. Engl.*, 2014, **53**, 4572-4577.

[10] Y. H. Chen, K. C. Tang, Y. T. Chen, J. Y. Shen, Y. S. Wu, S. H. Liu, C. S. Lee, C. H. Chen, T. Y. Lai, S. H. Tung, R. J. Jeng, W. Y. Hung, M. Jiao, C. C. Wu and P.

T. Chou, Insight into the mechanism and outcoupling enhancement of excimer-associated white light generation, *Chem. Sci.*, 2016, **7**, 3556-3563.

[11] H. Liu, X. Cheng, H. Zhang, Y. Wang, H. Zhang and S. Yamaguchi, ESIPT-active organic compounds with white luminescence based on crystallization-induced keto emission (CIKE), *Chem. Commun.*, 2017, **53**, 7832-7835.

[12] Z. Xie, C. Chen, S. Xu, J. Li, Y. Zhang, S. Liu, J. Xu and Z. Chi, White-light emission strategy of a single organic compound with aggregation-induced emission and delayed fluorescence properties, *Angew. Chem. Int. Ed. Engl.*, 2015, **54**, 7181-7184.

[13] C. Li, J. Liang, B. Liang, Z. Li, Z. Cheng, G. Yang and Y. Wang, An Organic Emitter Displaying Dual Emissions and Efficient Delayed Fluorescence White OLEDs, *Adv. Opt. Mater.*, 2019, **7**, 1801667.

[14] C. Zhou, S. Zhang, Y. Gao, H. Liu, T. Shan, X. Liang, B. Yang and Y. Ma, Ternary Emission of Fluorescence and Dual Phosphorescence at Room Temperature: A Single-Molecule White Light Emitter Based on Pure Organic Aza-Aromatic Material, *Adv. Funct. Mater.*, 2018, **28**, 1802407.

[15] Z. He, W. Zhao, J. W. Y. Lam, Q. Peng, H. Ma, G. Liang, Z. Shuai and B. Z. Tang, White light emission from a single organic molecule with dual phosphorescence at room temperature, *Nat. Commun.*, 2017, **8**, 416.

[16] J. A. Li, J. Zhou, Z. Mao, Z. Xie, Z. Yang, B. Xu, C. Liu, X. Chen, D. Ren, H. Pan, G. Shi, Y. Zhang and Z. Chi, Transient and Persistent Room-Temperature Mechanoluminescence from a White-Light-Emitting AIEgen with Tricolor Emission Switching Triggered by Light, *Angew. Chem. Int. Ed. Engl.*, 2018, **57**, 6449-6453.

[17] Y. Zhang, Y. Miao, X. Song, Y. Gao, Z. Zhang, K. Ye and Y. Wang, Single-Molecule-based White-Light Emissive Organic Solids with Molecular-Packing-Dependent Thermally Activated Delayed Fluorescence, *J. Phys. Chem. Lett.*, 2017, **8**, 4808-4813.

[18] B. Xu, H. Wu, J. Chen, Z. Yang, Z. Yang, Y. C. Wu, Y. Zhang, C. Jin, P. Y. Lu, Z. Chi, S. Liu, J. Xu and M. Aldred, White-light emission from a single heavy atom-free molecule with room temperature phosphorescence, mechanochromism and thermochromism, *Chem. Sci.*, 2017, **8**, 1909-1914.

[19] X. Ma, L. Jia, B. Yang, J. Li, W. Huang, D. Wu and W.-Y. Wong, A color-tunable single molecule white light emitter with high luminescence efficiency and ultra-long room temperature phosphorescence, *J. Mater. Chem. C*, 2021, **9**, 727-735.